ARTICLE NO. 80-4003

G80-009

A Statistical Method Applied to Pilot Behavior Analysis in Multiloop Systems

00017

Norihiro Goto*
Kyushu University, Fukuoka, Japan

A recently developed statistical method has been applied to the analysis of pilot control behavior in multiloop systems. The method utilizes the so-called autoregressive scheme, and produces analytical results in terms of root mean square values, power spectra, and pilot describing functions. The method is practical in that it manipulates operating records and it can check the validity of the assumed compensatory control system structure. To show the usage and feasibility of the method, the data from a series of moving-base simulator experiments have been analyzed by the method. Emphasis of the experiment was placed on the lateral-directional control of an aircraft in the landing approach phase under the influence of turbulence. The variation of pilot control behavior with respect to two experimental variables, the Dutch-roll damping ratio and the flight rules, is presented with the discussion as to the system structure and the limitations of the method. Since the application of the method to the field of pilot behavior analysis is quite new, the described method and the presented results are considered to help better analyze and understand pilot behavior in multiloop systems.

Introduction

GENERALLY it can be said that the pilot in control of an aircraft is a multivariable processor and controller. Understanding pilot control behavior in multiloop control situations is thus fundamental to properly interpreting pilot ratings and to analytically assessing aircraft handling qualities. As discussed in Ref. 1, however, there are a number of difficulties—instrumental, measurement, and analytical—in identifying pilot control behavior in multiloop situations. Because of the difficulties, a limited number of measurements pertinent to aircraft multiloop control have been conducted so far.[2-4]

As far as the analytical difficulty is concerned, recent development of systems theory and identification techniques seems to be encouraging us to go a step ahead into the area of identifying pilot control behavior in a certain class of multiloop systems. This work makes an attempt at applying a recently developed system identification method to a typical multiloop control phase of an aircraft. The identification method makes use of the so-called autoregressive (AR) scheme,[5-7] and has practical characteristics such that the identification is made by manipulating operating records only and that the method can examine the validity of the assumed multiloop structure. By the conventional spectral analysis technique, on the other hand, it is necessary to measure the externally injected noises and to have a full knowledge of the system structure.

As one of the flight phases where the pilot control behavior in multiloop situations can be readily determined, lateral-directional control of an aircraft in landing approach under the influence of turbulence is considered. In landing approach, tight control in multiloop fashion is required of the pilot to hold the aircraft on the proper course. In addition, the presence of turbulence should make his correction controls be applied almost continuously. The continuous nature of the pilot's control and the existence of random external noises make it possible to estimate the pilot linear dynamics.

Received December 5, 1978; revision received March 5, 1979.

Index category: Handling Qualities, Stability and Control.

*Associate Professor, Department of Aeronautical Engineering.

Using the landing approach phase and employing, as experimental variables, the Dutch-roll mode damping ratio and the flight rules, a series of simulator experiments was conducted by the use of a six-degree-of-freedom moving-base simulator. This paper first describes the identification method. Then it presents examples of the analyzed data in terms of root mean square values (rms), power spectra, and pilot describing functions. Based on the results, discussion is made of the identification method and its limitations.

System Model and the Analytical Method

Consider the typical compensatory control system shown in Fig. 1. Although we do not know the real system structure set up by the pilot, the model of Fig. 1 is considered to be a fairly general one comprising most of the multiloop system structures treated so far.[2,4,8] To the lateral-directional control in the landing approach phase by instrument flight rules (IFR) in the experiment of this work, it will be shown that the model of Fig. 1 may be applied.

Since there are two control variables and three independent controlled variables in the lateral-directional control system under consideration, the vectors $\pi(n)$ and $\Theta(n)$ $(n=1,2,\ldots,N)$ in Fig. 1 may be set as

$$\pi(n) = [\delta_w(n) \quad \delta_p(n)]^T \tag{1}$$

$$\Theta(n) = [\phi(n) \quad \psi(n) \quad \beta(n)]^T \tag{2}$$

where

$\delta_w(n)$ = pilot's wheel movements, deg
$\delta_p(n)$ = pilot's pedal movements, cm
$\phi(n)$ = bank angle output of the aircraft, deg
$\psi(n)$ = heading angle output of the aircraft, deg
$\beta(n)$ = sideslip angle output of the aircraft, deg

The superscript T in Eqs. (1) and (2) denotes the transpose.

The system equations that describe the model of Fig. 1 are

$$\pi(n) = [Y_\pi(B)]\Theta(n) + U_r(n) \tag{3a}$$

$$\Theta(n) = [G_c(B)]\pi(n) + U_g(n) \tag{3b}$$

where the relationship $\Theta_c = -\Theta$ is used with the command Θ_c assumed zero, and B is the backward shift operator,[5,9] $B^k y(n) = y(n-k)$. The matrices $[Y_\pi(B)]$ and $[G_c(B)]$

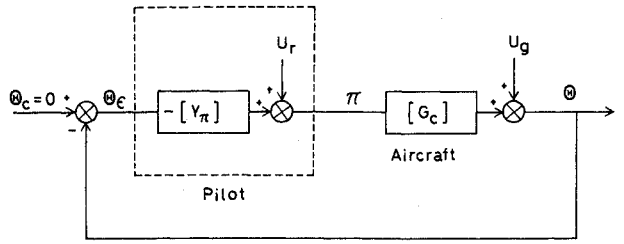

Fig. 1 A compensatory multiloop system structure for lateral-directional control.

represent the pilot dynamics and aircraft dynamics, respectively. They are defined, if we employ the definitions of Eqs. (1) and (2), as

$$-[Y_\pi(B)] = \begin{bmatrix} \delta_w/\phi & \delta_w/\psi & \delta_w/\beta \\ \delta_p/\phi & \delta_p/\psi & \delta_p/\beta \end{bmatrix} \tag{4}$$

$$[G_c(B)] = \begin{bmatrix} \phi/\delta_w & \phi/\delta_p \\ \psi/\delta_w & \psi/\delta_p \\ \beta/\delta_w & \beta/\delta_p \end{bmatrix} \tag{5}$$

where the component δ_w/ϕ, for example, is the pilot's wheel control transfer function to the bank angle input described in terms of the backward shift operator B. U_r in Eq. (3a) is the 2×1 pilot remnant vector and U_g in Eq. (3b) is the 3×1 external noise vector. The feedback system model of Eqs. (3a) and (3b) was first studied by Akaike.[10]

We set assumptions as follow:

1) $\pi(n)$, $\Theta(n)$, $U_r(n)$ and $U_g(n)$ are all stationary and zero mean.

2) The feedback system of Fig. 1 is stable.

3) The noise vectors $U_r(n)$ and $U_g(n)$ are uncorrelated with each other.

4) The noise vectors satisfy

$$U_r(n) = [H_r(B)]\,w_r(n) \tag{6a}$$

$$U_g(n) = [H_g(B)]\,w_g(n) \tag{6b}$$

where $[H_r(B)]$ and $[H_g(B)]$ are 2×2 and 3×3 nonsingular matrices, respectively, and $w_r(n)$ and $w_g(n)$, two and three dimensional, respectively, are white noise vectors such that

$$E[w_r(n)\cdot w_g^T(n+l)] = 0 \quad \text{(zero matrix) for all } l \tag{7}$$

E in Eq. (7) denotes expectation.

5) $[H_r(0)]$ and $[H_g(0)]$ in Eqs. (6a) and (6b) are such that $[H_r(0)] = I_2$, $[H_g(0)] = I_3$, with I_k denoting the k-dimensional unit matrix.

6) Either $[Y_\pi(0)]$ or $[G_c(0)]$ is zero (matrix).

Assumption 3 is the key assumption associated with the model of Fig. 1. The prewhitening operation, Eqs. (6a) and (6b), is necessary since the least-squares algorithm is used later to estimate the unknown parameters of AR models. Also the nonsingular nature of $[H_r(B)]$ and $[H_g(B)]$ requires that there be two and three statistically independent noise sources in $w_r(n)$ and $w_g(n)$, respectively. Equation (7) is equivalent to the key assumption 3 and is used to check whether or not the model of Fig. 1 is appropriate. The assumptions 5 and 6 are not general ones,[10] but for the structure of Fig. 1 they are considered practical. Since the pilot has a reaction time lag, it usually holds that $[Y_\pi(0)] = 0$. The presence of $[G_c(0)]$ needs a slight modification of the procedure that follows. However, the influence of $[G_c(0)]$ proves to be small, if we set $[G_c(B)]$ as Eq. (5).

From the system equations Eqs. (3a) and (3b) we obtain

$$\begin{bmatrix} \pi(n) \\ \Theta(n) \end{bmatrix} = \begin{bmatrix} L_{11}(B) & L_{12}(B) \\ L_{21}(B) & L_{22}(B) \end{bmatrix} \begin{bmatrix} w_r(n) \\ w_g(n) \end{bmatrix} \tag{8}$$

where

$$L_{11}(B) = (I_2 - [Y_\pi(B)][G_c(B)])^{-1}[H_r(B)] \tag{9a}$$

$$L_{12}(B) = (I_2 - [Y_\pi(B)][G_c(B)])^{-1}[Y_\pi(B)][H_g(B)] \tag{9b}$$

$$L_{21}(B) = (I_3 - [G_c(B)][Y_\pi(B)])^{-1}[G_c(B)][H_r(B)] \tag{9c}$$

$$L_{22}(B) = (I_3 - [G_c(B)][Y_\pi(B)])^{-1}[H_g(B)] \tag{9d}$$

The inverse matrices are assumed to exist. Suppose that Eq. (8) has been determined by manipulating the observed data $\pi(n)$ and $\Theta(n)$. Then Eqs. (9a-9d) may be solved for the unknowns $[Y_\pi(B)]$, $[G_c(B)]$, $[H_r(B)]$, and $[H_g(B)]$. The pilot transfer function matrix is given by

$$[\tilde{Y}_\pi(B)] = L_{12}(B)\cdot L_{22}^{-1}(B) \tag{10}$$

Frequency response functions can be computed by replacing B in Eq. (10) by $\exp(-j\omega T_s)$ with T_s as the sampling interval and j as $\sqrt{-1}$.

Autoregressive modeling method[5-7] can be used to develop the form Eq. (8). By setting

$$X(n) = [\pi^T(n)\Theta^T(n)]^T$$

$$W(n) = [w_r^T(n)\,w_g^T(n)]^T$$

the multidimensional AR-model is obtained in the form

$$X(n) = \sum_{k=1}^{K} A(k)X(n-k) + W(n) \tag{11}$$

with

$$E[W(n)] = 0 \quad \text{(zero vector)} \tag{12a}$$

$$E[W(n)\cdot X^T(n-l)] = 0 \quad \text{(zero matrix) for } l \geq 1 \tag{12b}$$

$$E[W(n)\cdot W^T(l)] = \delta_{n,l}\Sigma_w \tag{12c}$$

where $\delta_{n,l} = 1$ $(n=l)$, $\delta_{n,l} = 0$ $(n\neq l)$, and Σ_w is the covariance matrix of $W(n)$. The estimation of the AR coefficient matrix $A(k)$ is made by the use of the recursive computational algorithm of the least squares based on the formulas developed by Whittle.[6,7] The order K of Eq. (11) can be determined through the objective judgment criterion multiple final prediction error[7] or Akaike's information criterion.[11]

From Eq. (11) we have

$$X(n) = [I_5 - A(B)]^{-1}W(n) \tag{13}$$

which is of the form of Eq. (8). In Eq. (13)

$$A(B) = \sum_{k=1}^{K} A(k)B^k \tag{14}$$

If the system structure is as shown in Fig. 1, it is necessary that Eq. (7) be satisfied. We first normalize the estimated Σ_w in Eq. (12). The element of the normalized Σ_w is given by $\epsilon_{ij} = \sigma_{ij}/\sqrt{\sigma_{ii}\sigma_{jj}}$ where σ_{ij} is the element of Σ_w. ϵ_{ij} is the correlation coefficient between w_i and w_j, w_i being the ith component of $W(n)$. Thus, to satisfy Eq. (7), ϵ_{ij}'s ($i=1,2$, $j=3,4,5$ and $i=3,4,5$, $j=1,2$) must be zero, or small compared to 1.0 in the practical sense.

Once the AR-model of Eq. (11) is fitted to the given data, the power spectral density matrix, $P_x(j\omega)$, of the vector $X(n)$ is given by

$$P_x(j\omega) = T_s[A(j\omega)]^{-1}\Sigma_w[\overline{A^T(j\omega)}]^{-1} \tag{15}$$

where

$$A(j\omega) = \sum_{k=0}^{K} A(k)\exp(-j\omega k)$$

with $A(0) = -I_5$, and $\overline{A(j\omega)}$ is the complex conjugate of $A(j\omega)$.

When Σ_w is diagonal, meaning that the components of $W(n)$ are mutually independent, we may arrive at a simple expression which gives the indication of the linear coherency characteristics as

$$r_{ij}(j\omega) = q_{ij}(j\omega)/p_{ii}(j\omega) \tag{16}$$

where $p_{ii}(j\omega)$ is the power spectrum of the ith component of the vector $X(n)$, and $q_{ij}(j\omega) = |[A(j\omega)]_{ij}^{-1}|^2\sigma_{jj}$. $[A(j\omega)]_{ij}^{-1}$ is the (i,j) component of $[A(j\omega)]^{-1}$, and σ_{jj} is the (j,j) component of Σ_w. $r_{ij}(j\omega)$ shows the contribution in power of the jth noise source to the power of the ith component of $X(n)$, and

$$\sum_{j=1}^{5} r_{ij}(j\omega) = 1 \tag{17}$$

This quantity is called the relative power contribution, and it is worth checking even when the off-diagonal elements of Σ_w are not zero but practically small; i.e., the off-diagonal elements of the normalized Σ_w are substantially smaller than 1.0.

The AR scheme has recently drawn much attention from various fields, and its applications can be found in the literature of Refs. 11 and 12. A credibility study and an application to the analysis of pilot control behavior in single and multiloop systems are reported in Refs. 13 and 14.

Experiment

A series of simulator experiments was conducted, using a six-degree-of-freedom moving-base simulator.[15] The simulated flight configuration of final landing approach is visualized in Fig. 2, where V_0, H_0, and γ_0 are the initial conditions and are listed in Table 1 together with the dimensions and the lateral-directional stability data of the simulated aircraft, a twin-engined jet transport of medium size. Three kinds of the Dutch-roll mode damping ratio, as one of the two experimental variables, were realized by adjusting the variable gain level of the yaw damper, which was incorporated in the stability augmentation system (SAS) of the aircraft and utilized the washed-out yaw rate feedback to rudder. The transfer function of the washout had two simple poles with time constants 0.3 1/s and 7.0 1/s. The values of the yaw damper gain level, denoted by G_1, are shown in Table 2 together with the resulting dynamic characteristics of lateral-directional modes. The employment of the Dutch-roll

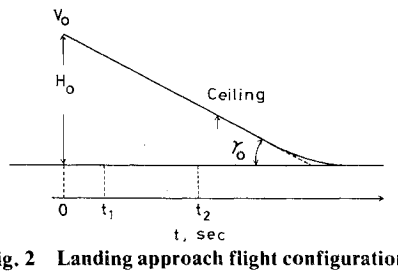

Fig. 2 Landing approach flight configuration.

Table 1 Flight loading conditions and stability derivative data

Aircraft dimensions	Initial conditions
V_0 = 130 knots	W = 43,100 kg(95,000 lb)
H_0 = 396 m (1300 ft)	S = 91.0 m^2 (980 ft^2)
γ_0 = −3.0 deg	b = 28.3 m (93 ft)
α_0 = 1.2 deg	I_x = 51,800 kg-m-s^2 (375,000 slug-ft^2)
δ_f = 40 deg (flap angle)	I_z = 166,000 kg-m-s^2 (1,200,000 slug-ft^2)
Ceiling = 91 m(300 ft)	I_{xz} = 6640 kg-m-s^2 (48,000 slug-ft^2)

Stability derivaties (body axis)

Y_v = −0.1432 1/s	N_r = −0.2321 1/s
L_β = −4.689 1/s^2	Y_{δ_a} = 0.0004 1/s
N_β = 0.9770 1/s^2	L_{δ_a} = 0.9675 1/s^2
Y_p = 0.0081	N_{δ_a} = 0.0291 1/s^2
L_p = −1.766 1/s	Y_{δ_r} = 0.0365 1/s
N_p = −0.1926 1/s	L_{δ_r} = 0.4093 1/s^2
Y_r = 0.0	N_{δ_r} = −0.6653 1/s^2
L_r = 1.007 1/s	

Data acquisition

T_s (sampling time) = 0.052 s
t_1 = 20 s, t_2 = 82.4 s

damping ratio as an experimental variable is based on the past flight experimental result that the Dutch-roll mode damping ratio has remarkable influence on pilot ratings and control behavior when the undamped natural frequency of the mode is low.[16]

Each case of the Dutch-roll damping ratio was flown both by instrument flight rules (IFR) and visual flight rules (VFR), flight rules being another experimental variable. Thus, the total number of the runs was six as seen in Table 3, where the pilot rating, based on the Cooper-Harper scale,[17] was given to each run as shown. Incidentally, the pitch SAS was kept on throughout the experiment to make the effect of longitudinal control on lateral-directional control as small as possible. For IFR runs a ceiling was set above which the pilot was required to fly by IFR. The position of the ceiling is shown in Fig. 2, and its altitude in Table 1. The analyzed data are all for the time interval between t_1, a while after the initiation, and t_2, a while before crossing the ceiling for IFR runs, thus avoiding the inclusion of the transitional effects in the analysis. The sampling time and the values for t_1 and t_2 are shown in Table 1.

The turbulence simulated in the experiment utilized the one-dimensional spectral density functions of the Dryden form. The method to generate the turbulence was based on Refs. 18 and 19 but with a modification that three statistically independent noise sources were used for the lateral turbulence components. One point to note is that the characteristics of the simulated turbulence were a function of the altitude as a result of employing the hypothesis of the two-dimensional isotropy. Thus, strictly speaking, stationarity on which the analytical method of this work is based does not hold along the flight path. The length of the time sector used for the analysis (from t_1 to t_2), however, is not considered to be long enough to make it necessary to take into account the nonstationarity. See Ref. 20, for example, for the change in the turbulence spectral form with respect to the turbulence scale. The turbulence scale L_w at the middle point between t_1 and t_2 was approximately 180 m (600 ft). The intensity of the turbulence, which is represented by the rms value of the vertical component w_g (i.e., σ_w), was set at 0.9 m/s (3 fps) throughout the experiment.

Table 2 Values of the yaw damper gain and the resulting dynamic mode characteristics

Case	G_I	ζ_D[a]	ω_{nD}[b], rad/s	τ_R[c], s	τ_s[d], s	$\lvert\phi/\beta\rvert_d$
A	0	0.0166	1.28	0.479	220	1.70
B	−0.07	−0.0210	1.28	0.479	219	1.51
C	0.68	0.366	0.943	0.484	232	2.65

[a] ζ_D = Dutch-roll mode damping coefficient.
[b] ω_{nD} = Dutch-roll mode undamped natural frequency.
[c] τ_R = roll mode time constant.
[d] τ_s = spiral mode time constant.

Table 3 Flight configurations and pilot ratings[a]

Configuration	Flight rule	Yaw damper gain G_I	Turbulence σ_w, m/s	Pilot rating
I	VFR	0	0.9	3.0
II	IFR	0	0.9	4.0
III	VFR	−0.07	0.9	7.0
IV	IFR	−0.07	0.9	8.0-9.0
V	IFR	0.68	0.9	2.0
VI	VFR	0.68	0.9	2.0

[a] Pitch-SAS on for every configuration; neither head wind nor crosswind exists; all moving base.

Table 4 An example of the normalized noise covariance matrix for an IFR flight (configuration II)

	δ_w	δ_p	ϕ	ψ	β
δ_w	0.1000000D 01	−0.5924826D-01	0.2608771D-01	0.1600583D 00	0.8465099D-01
δ_p	−0.5924826D-01	0.1000000D 01	−0.3005102D-02	0.1041485D 00	0.4834996D-01
ϕ	0.2608771D-01	−0.3005102D-02	0.1000000D 01	−0.3449463D 00	0.2673959D-01
ψ	0.1600583D 00	0.1041485D 00	−0.3449463D 00	0.1000000D 01	0.1253667D 00
β	0.8465099D-01	0.4834996D-01	0.2673959D-01	0.1253667D 00	0.1000000D 01

The pilot who participated in this experiment was an experienced instrument-rated pilot, having had more than 2500 hours of flight time in single and multiengine jet aircraft. In the experiment, some fixed-base and moving-base runs with and without turbulence inputs were first made for familiarization with the aircraft dynamics. Then, six preliminary runs including each configuration of Table 3 preceeded the six runs for data taking. The pilot was informed, before each run, of the change of the dynamics but not how.

Measurements were made of the pilot's outputs and the aircraft outputs as shown in Eqs. (1) and (2). The deviation angle y_ϵ, from the localizer beam was also measured as a quantity to show the performance of the run. The measured data were sampled, stored on magnetic tapes and processed digitally. Note that δ_w and δ_p are wheel displacement angle and pedal travel, respectively, instead of the forces applied by the pilot to wheel and pedal. Therefore, the pilot dynamics shown later may contain the wheel and pedal dynamics.

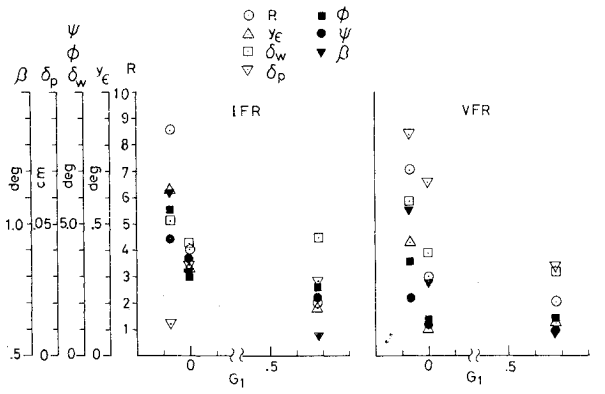

Fig. 3 Variation of pilot ratings and the rms values of the pilot control outputs and the aircraft outputs, R = pilot rating.

Results and Discussion

The data obtained from the simulator experiments were analyzed by the previously described method, setting the vectors π and Θ as Eqs. (1) and (2). Some of the results are shown and discussed in this section.

First of all, let us look at Fig. 3, which shows the variation of pilot ratings and rms values with respect to the change in yaw damper gain G_I. The trend of the pilot rating variation is similar in both IFR and VFR, although the ratings for VFR flights are better than those for IFR flights. Note the clear difference in pedal usage between IFR and VFR. For IFR flights, it may as well be said that almost no pedal pressure was applied. This situation is also indicated in Fig. 4, which shows the relative power contribution for the power spectra of the pilot control outputs [see Eq. (16) for definition] for configuration II of Table 3. In Fig. 4, $\delta_p - \phi$, for example, means the power content that responded, in the linear sense, to the external disturbance in the total power of δ_p at a particular frequency. If the pilot controls are responding well to the external disturbances, the power contents δ_w − or δ_p − ϕ, ψ, β in the total power of δ_w or δ_p must be large. The lower diagram of Fig. 4 shows that more than 70% of the power of δ_p, which is quite small in itself as Fig. 5 for the same configuration shows, is just the noise generated by the pilot himself. Thus, the pedal usage for IFR flights in this experiment may be considered insignificant. This difference of pedal usage between IFR and VFR seems to come mainly from the pilot's information-receiving situation. According to

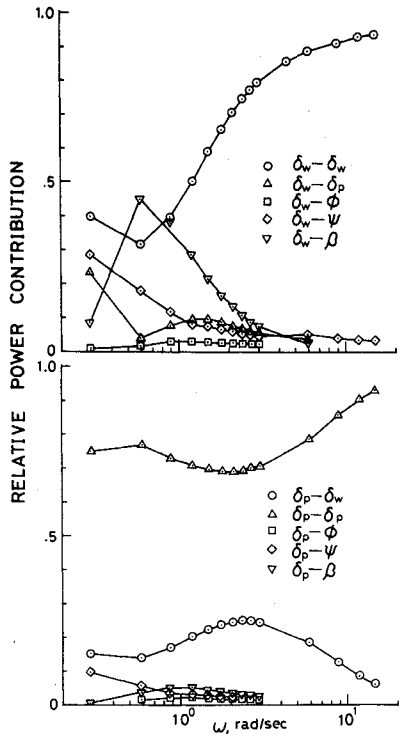

Fig. 4 Relative power contribution—configuration II of Table 3.

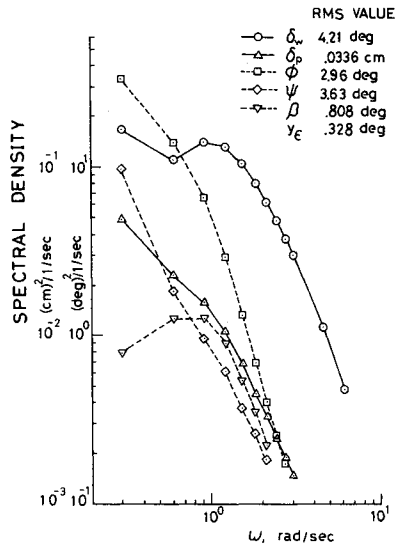

Fig. 5 Power spectra of the pilot controls and the aircraft outputs—configuration II.

the pilot comments, by VFR the pilot could acquire information concerning bank angle, heading motion, and lateral deviation by referring to the runway and horizon as seen head up, whereas under IFR continuous reference to the heading indicator to detect yaw rate was difficult. Consequently, VFR could allow the pilot to use the pedals more effectively than IFR for directional control.

Figure 5 shows an example of the power spectra of the pilot controls and aircraft outputs for an IFR configurtion. Figure 6, which is for configuration I, a VFR case, is presented for comparison with the IFR case. Generally they show the feature that the spectrum of wheel movements has a peak at the Dutch-roll frequency. This may imply that the pilot's concern was in the control of the Dutch-roll mode. It is also seen from Figs. 5 and 6 that the power content of bank angle motion around the Dutch-roll frequency is larger than those

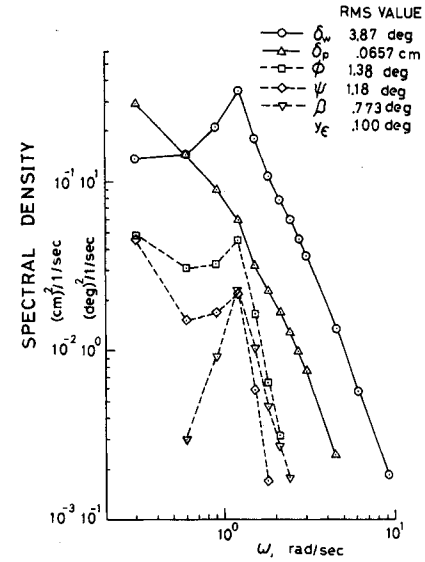

Fig. 6 Power spectra of the pilot controls and the aircraft outputs—configuration I.

of the other aircraft outputs around the same frequency range, indicating that the influence of turbulence was biggest on the bank angle motion of the aircraft around the Dutch-roll frequency.

Table 4 shows the normalized noise covariance matrix for configuration II, an IFR case, as an example to check if the system structure model of Fig. 1 is appropriate. It may be seen that the components in the brackets in the matrix of Table 4, showing the correlation between the pilot remnants and the turbulence-induced noises, are small compared to 1.0. Thus, the condition of Eq. (7) is approximately satisfied. It may be said that the system model of Fig. 1 is applicable to this particular configuration. The correlation situations are almost the same for the other IFR configurations also. In the simulation portion of this work, the aircraft was aligned with the localizer beam at the initial condition. Furthermore, no crosswind was included in the turbulence. It may be said, therefore, that the pilot's role was mainly to keep ϕ, ψ, and β zero, thereby also making the lateral deviation as small as possible. Since the lateral deviation y is linearly related to ψ and β, if small-disturbance equations of motion are considered, as[21]

$$y_\epsilon = \frac{1}{V_0}\frac{dy}{dt} = \psi\cos\gamma_0 + \beta \tag{18}$$

the lateral deviation is controlled through ψ and β.

On the other hand, the system model of Fig. 1 was not found applicable to VFR configurations, since large correlation existed between the pilot remnants and the turbulence-induced noises. No appropriate system structure for VFR flights has yet been identified. A conjecture that can be made is that in VFR the pilot could add a feedforward loop to compensate for the effects of turbulence. If such a feedforward loop was present, the turbulence-induced noises might directly affect the pilot controls, thereby producing large correlation with the pilot remnants. By the analytical method described in this work, it is not possible to detect the dynamics in the feedforward loop. More consideration on the system structure and the refinement of the analytical method are necessary.

Figures 7 and 8 show the examples of the wheel-related frequency response functions of the pilot for IFR cases with the use of the model of Fig. 1; Fig. 7 is for a positive Dutch-roll damping case and Fig. 8 for a negative Dutch-roll damping case. In Fig. 7, first of all, the frequency response

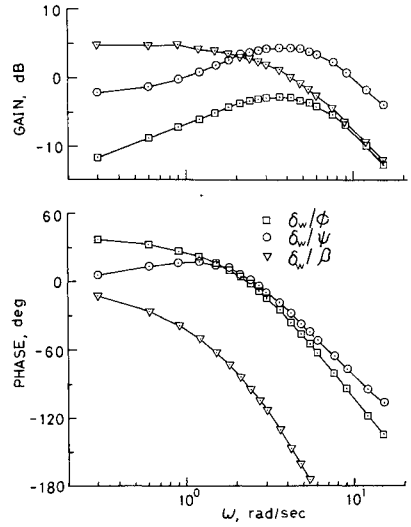

Fig. 7 Wheel-related frequency response functions of the pilot—configuration II.

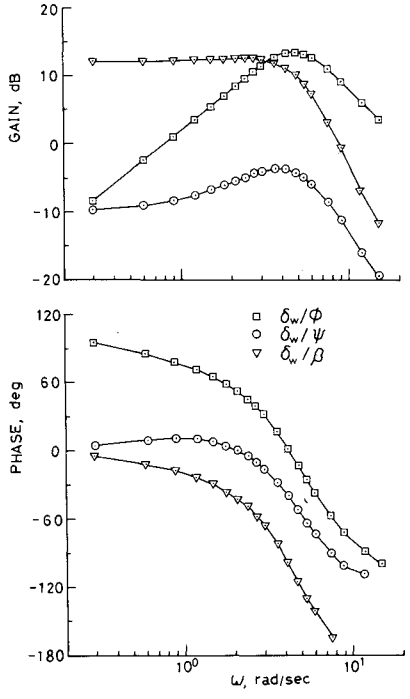

Fig. 8 Wheel-related frequency response functions of the pilot—configuration IV.

functions δ_w/ϕ and δ_w/ψ exhibit lead characteristics. δ_w/β is of lag control but with fairly large static gain. It is known that the rolling velocity feedback to aileron increases $1/\tau_R$, the roll subsidence break frequency, and it in turn improves the aircraft response to rolling gust. Thus, the lead characteristics in δ_w/ϕ are understandable. Since the simulated aircraft with yaw damper off has fairly large L_β and low Dutch-roll natural frequency and damping, the bank angle response to side gust β_g must be fairly large, as also indicated by the modal response ratio $|\phi/\beta|_d$ in Table 2. Although the phase diagrams of the frequency response functions are shown ignoring the associated signs, δ_w/β's in Figs. 7 and 8 have minus signs, meaning that the phase should start from ± 180 deg, if the sign is explicitly exhibited. A negative gain in $\beta \rightarrow \delta_w$ feedback works so as to decrease the magnitude of L_β and thus works to decrease the bank angle response to side gust.[22] This may explain the large static gain of δ_w/β. Also note that Fig. 4 shows a large wheel response to the noise in β. Combined with the negative gain feedback of $\beta \rightarrow \delta_w$, and taking advantage of the favorable aileron yaw of the model aircraft the lead characteristics in δ_w/ψ are considered to have worked so as to augment the Dutch-roll damping.

For the negative Dutch-roll damping case, configuration IV, it is seen that similar but more intensive controls are employed. δ_w/ϕ in Fig. 8 is almost a pure differentiator, and the static gain of δ_w/β is higher than in the previous case. The pilot comment for this case, saying "Tried to damp out roll by wheel, no rudder pressure," is considered to be well reflected in Fig. 8. Taking into account the fact that the lead control in δ_w/ψ is not so remarkable as seen in Fig. 8 and pedal pressure is almost zero, it is to be noted that the pilot does not seem to be taking positive action to stabilize the Dutch-roll mode. The pilot was not informed that configuration IV had unstable Dutch-roll mode. More training before the data taking may have been necessary so that he could work out a suitable control technique to stabilize the Dutch-roll mode. For VFR configurations, on the other hand, the increase in the rms value of pedal usage following the deterioration of the Dutch-roll damping suggests that more effective controls were employed by the pilot to augment the stability.

Since pedal usage seems to be insignificant for IFR runs, no pedal-related frequency response functions are shown. However, the three pedal-related frequency response functions, together with the three wheel-related ones, make up the complete matrix of Eq. (4).

Summarizing the discussion made hitherto, it can be said that considerable insight into pilot control behavior can be obtained by collecting such statistical data as analyzed and shown here. However, as can be seen from Fig. 4, only 50% or less in the total power of the pilot control efforts can be accounted for by the linear model of the type used here. In order to design a control system, effective and suitable for the pilot, it may be necessary to consider the content of the power regarded as remnants by the linear model. In the analysis of this work, the pilot control characteristics concerning the path or the lateral deviation was not included, although it is recognized important. However, as can be considered from Eq. (18), the characteristics concerning the path control may be included in those concerning ψ and β controls. The transfer function δ_w/y_ϵ, for example, may be a linear combination of δ_w/ψ and δ_w/β. The function form and the method to estimate δ_w/y_ϵ from δ_w/ψ and δ_w/β are to be developed in the future.

Conclusions

An analytical procedure is described for studying multidimensional pilot control behavior. The procedure utilizes the autoregressive modeling method under the assumption of a compensatory closed-loop system structure. Results are produced in terms of root mean square values, power spectra, pilot describing functions, and an indication of linear coherency characteristics. The procedure is practical in that it manipulates operating records only and the validity of the system structure can be checked. It may be applied to realistic situations where it is difficult to measure the random external disturbances. It is also shown, however, that if the system structure is not the usual compensatory closed system it is difficult, at present, to identify an appropriate structure.

The procedure is applied in this work to the analysis of the lateral-directional control behavior of a pilot in the landing approach phase under the influence of turbulence. The analysis shows that for IFR the ordinary compensatory system model may be applicable, while for VFR the system model is to be pursued further. The effects of the Dutch-roll mode damping ratio are clearly seen in the results. Pilot behavior and its correlation with the handling quality parameters may be further defined by this line of approach.

Acknowledgments

This work was supported by the Grant-in-Aid for Scientific Research. The experiment of this work was conducted at the

NASA Ames Research Center. The author is indebted to J.A. Franklin for his encouragement and discussion on this work, and to R.S. Bray and C.C. Mattraw for their participation in the experiment.

References

[1] McRuer, D.T., "Development of Pilot-in-the-Loop Analysis," *Journal of Aircraft,* Vol. 10, Sept. 1973, pp. 515-524.

[2] Stapleford, R.L., McRuer, D.T., and Magdaleno, R.E., "Pilot Describing Function Measurements in a Multiloop Task," *IEEE Transactions on Human Factors and Electronics,* Vol. HFE-8, June 1967, pp. 113-125.

[3] Weir, D.H. and McRuer, D.T., "Pilot Dynamics for Instrument Approach Task: Full Panel Multiloop and Flight Director Operations," NASA CR-2019, 1972.

[4] Beppu, G., "A Study of Pilot Behavior During Controlling the Lateral-Directional Motion of Airplanes in Turbulent Air," NASA TM X-62,464, 1975, pp. 625-644.

[5] Box, G.E.P. and Jenkins, G.M., *Time Series Analysis, Forecasting and Control,* Holden-Day, San Francisco, 1970.

[6] Whittle, P., "On the Fitting of Multivariate Autoregressions and the Approximate Canonical Factorization of a Spectral Density Matrix," *Biometrica,* Vol. 50, 1963, pp. 129-134.

[7] Akaike, H., "Autoregressive Model Fitting for Control," *Annals of the Institute of Statistical Mathematics,* Vol. 23, 1971, pp. 163-180.

[8] Todosiev, E.P., "Human Performance in a Cross-Coupled Tracking System," *IEEE Transactions on Human Factors and Electronics,* Vol. HFE-8, Sept. 1967, pp. 210-217.

[9] Shinners, S.M., "Modeling of Human Operator Performance Utilizing Time Series Analysis," *IEEE Transactions on Systems, Man, and Cybernetics,* Vol. SMC-4, Sept. 1974, pp. 446-458.

[10] Akaike, H., "On the Use of a Linear Model for the Identification of Feedback Systems," *Annals of the Institute of Statistical Mathematics,* Vol. 20, 1968, pp. 425-439.

[11] Akaike, H., "Canonical Correlation Analysis of Time Series and the Use of an Information Criterion," *System Identification: Advances and Case Studies,* edited by R.K. Mehra, and D.G. Lainiotis, Academic Press, New York, 1976, pp. 27-96.

[12] Akaike, H., "On Newer Statistical Approaches to Parameter Estimation and Structure Determination," *Proceedings of the 7th IFAC World Congress,* Helsinki, Finland, June 1978, pp. 1877-1884.

[13] Goto, N., "A Statistical Approach to the Analysis of Pilot Behavior in Multiloop Systems," NASA TM X-73,170, 1976, pp. 501-527.

[14] Tanaka, K., Goto, N., and Washizu, K., "A Comparison of Techniques for Identifying Human Operator Dynamics Utilizing Time Series Analysis," NASA TM X-73,170, 1976, pp. 673-693.

[15] Sinacori, J.B., Stapleford, R.L., Jewell, W.F., and Lehman, J.M., "Researcher's Guide to the NASA Ames Flight Simulator for Advanced Aircraft," NASA CR-2875, 1977.

[16] Franklin, J.A., "Turbulence and Lateral-Directional Flying Qualities," NASA CR-1718, 1971.

[17] Cooper, G.E. and Harper, R.P., Jr., "The Use of Pilot Rating in the Evaluation of Aircraft Handling Qualities," NASA TN D-5153, 1969.

[18] McFarland, R.E., "A Standard Kinematic Model for Flight Simulation at NASA-Ames," NASA CR-2497, 1975.

[19] Parris, B.L., "Modeling Turbulence for Flight Simulations at NASA Ames," Computer Science Corp., CSCR No. 4, 1975.

[20] Chalk, C.R., et al., "Background Information and User Guide for MIL-F-8785B(ASG)," Air Force Flight Dynamics Laboratory, Wright Patterson Air Force Base, Ohio, AFFDL-TR-69-72, 1969, p. 427.

[21] Etkin, B., *Dynamics of Flight,* John Wiley and Sons, Inc., New York, 1963.

[22] McRuer, D., Ashkenas, I., and Graham, D., *Aircraft Dynamics and Automatic Control,* Princeton University Press, Princeton, N.J., 1973, pp. 458-490.